Element-specific study of the temperature dependent magnetization of Co-Mn-Sb thin films

J. Schmalhorst,* D. Ebke, M. Meinert, A. Thomas, and G. Reiss
Thin Films and Physics of Nanostructures, Department of Physics, Bielefeld University, 33501 Bielefeld, Germany

E. Arenholz
Lawrence Berkeley National Laboratory, Berkeley, CA 94720, USA
(Dated: January 13, 2009)

Magnetron sputtered thin Co-Mn-Sb films were investigated with respect to their element-specific magnetic properties. Stochiometric $Co_1Mn_1Sb_1$ crystallized in the $C1_b$ structure has been predicted to be half-metallic and is therefore of interest for spintronics applications. It should show a characteristic antiferromagnetic coupling of the Mn and Co magnetic moments and a transition temperature T_C of about 480K. Although the observed transition temperature of our 20nm thick $Co_{32.4}Mn_{33.7}Sb_{33.8}$, $Co_{37.7}Mn_{34.1}Sb_{28.2}$ and $Co_{43.2}Mn_{32.6}Sb_{24.2}$ films is in quite good agreement with the expected value, we found a ferromagnetic coupling of the Mn and Co magnetic moments which indicates that the films do not crystallize in the $C1_b$ structure and are probably not fully spin-polarized. The ratio of the Co and Mn moments does not change up to the transition temperature and the temperature dependence of the magnetic moments can be well described by the mean field theory.

PACS numbers: 75.70.-i, 78.70.Dm, 85.75.-d

I. INTRODUCTION

Fully spin-polarized so called half-metallic ferromagnetic materials are of highest interest for spintronic applications such as nonvolatile memories[1] or field programmable logic devices[2,3]. They are characterized by a gap in the density of states (DOS) for minority (or majority) electrons at the Fermi energy E_F. This half-metallicity has been predicted theoretically for some half and full Heusler compounds[4–8]. Moreover, a strong influence of the atomic structure on their electronic properties is expected. Full Heusler alloys X_2YZ often crystallize in the $L2_1$ structure which consists of four interpenetrating fcc sublattices (the unit cell is that of a fcc lattice with four atoms as basis: X at (000) and $(\frac{1}{2}\frac{1}{2}\frac{1}{2})$, Y at $(\frac{1}{4}\frac{1}{4}\frac{1}{4})$ and Z at $(\frac{3}{4}\frac{3}{4}\frac{3}{4})$ in Wyckoff coordinates[6]). The $C1_b$ structure of half Heusler alloys XYZ is comparable to the $L2_1$ structure, but with a vacant site at $(\frac{1}{2}\frac{1}{2}\frac{1}{2})$ instead of X.

The structural, magnetic and electronic properties of the half Heusler compound CoMnSb are controversial in the literature. Galanakis[9] assumed CoMnSb to crystallize in the $C1_b$ structure (X=Co, Y=Mn and Z=Sb). Using a full-potential version of the screened KKR Green function method he calculated a total CoMnSb spin magnetic moment of almost $3\mu_B$ per formula unit (f.u.). The Mn ($3.18\mu_B$) and the Co ($-0.13\mu_B$) spin moments are antiferromagnetically aligned and half-metallicity with a large spin-down gap ($\sim 1eV$) was proposed.

Experimentally, however, a total magnetic moment of about $4\mu_B$ / f.u. was observed[10], which could be explained by Tobola *et al.*[11] by assuming a more complex structure (space group $Fd\bar{3}m$) originally proposed by Senateur *et al.*[12] in 1972. The calculated mean Mn and Co magnetic moments are $3.51\mu_B$ and $0.48\mu_B$, respectively for this structure and ferromagnetic coupling is expected. Although CoMnSb crystallized in this structure should still be half-metallic, the spin-down gap is predicted to be very narrow in contrast to the large gap derived from calculations by Galanakis[9] for the $C1_b$ structure.

Assuming a disordered $L2_1$ structure - the two X sublattices were occupied by 50% Co and 50% vacant sites and the Y and Z sublattices by Mn and Sb, respectively - Kaczmarska *et al.*[13] could also reproduce a magnetic moment of nearly $4\mu_B$ / f.u. by KKR-CPA calculations. Again a ferromagnetic coupling of Mn ($3.60\mu_B$) and Co ($0.30\mu_B$) was derived, but half-metallicity disappeared in this case. Very recently, Ksenofontov *et al.*[14] used NMR and Mössbauer spectroscopy to study bulk CoMnSb, they assigned it to the space group $Fm\bar{3}m$ and proposed that the CoMnSb structure can be presented as an alternation of Co_2MnSb and MnSb structural units with a Co moment of $0.55\mu_B$ and a mean Mn moment of $3.48\mu_B$. Again, half-metallicity is not predicted for this structure type.

To unambiguously determine the magnetic properties of these intriguing systems, we investigated the temperature dependence of magnetic moments of thin $Co_{32.4}Mn_{33.7}Sb_{33.8}$, $Co_{37.7}Mn_{34.1}Sb_{28.2}$ and $Co_{43.2}Mn_{32.6}Sb_{24.2}$ films grown on a Cu / Ta / V buffer in an element specific way using soft x-ray spectroscopy.

II. EXPERIMENTAL

The samples were deposited at room temperature by DC-magnetron sputtering on 200nm thick Si_3N_4 membranes from Silson Ltd., UK. The membranes (3mm×3mm) were supported by a 200μm thick Si frame (10mm×10mm). The surface roughness of the

Si_3N_4 measured on the supporting Si frame by atomic force microscopy was 0.6nm RMS. The 20nm thick Co-Mn-Sb films were deposited on a Cu^{80nm} / Ta^{5nm} / V^{10nm} buffer. Three different sputter targets were used to synthesize nearly stochiometric $Co_{32.4}Mn_{33.7}Sb_{33.8}$ (sample I, composition of target: $Co_{29.0}Mn_{32.1}Sb_{38.9}$) and sligthly off-stochiometric $Co_{37.7}Mn_{34.1}Sb_{28.2}$ (sample II, composition of target: $Co_{33.3}Mn_{33.3}Sb_{33.3}$) and $Co_{43.2}Mn_{32.6}Sb_{24.2}$ (sample III, composition of the target: $Co_{35.1}Mn_{29.4}Sb_{35.5}$). All stacks were capped by a thin Al layer (sample I: d_{Al}=1.6nm; sample II and III: d_{Al}=2.0nm) to prevent oxidation of the Co-Mn-Sb. After deposition the samples were annealed in vacuum at an optimized annealing temperature of 300°C to improve the structural quality of the films[15].

Temperature dependent x-ray absorption (XA) spectroscopy and x-ray magnetic circular dichroism (XMCD) measurements were performed at beamline (BL) 6.3.1 and BL 4.0.2 at the Advanced Light Source in Berkeley, USA. The Co- and Mn-L edges were investigated in bulk-sensitive transmission mode[16]. The x-rays angle of incidence with respect to the sample surface was 45^o at BL 6.3.1 and normal to the sample surface at BL 4.0.2. XMCD spectra were obtained by applying a magnetic field (BL 6.3.1: max. ± 0.2T; BL 4.0.2: max. ±0.68T) along the x-ray beam direction using elliptically polarized radiation with a degree of polarization of +75% (BL 6.3.1) and ±90% (BL 4.0.2). The sample temperature was varied between 15K and 450K. I^+ and I^- denote the transmission spectra for parallel and anti-parallel orientation of photon spin and magnetic field. The transmitted x-rays were detected by a photo-diode. I_0 denotes the spectrum of the direct x-ray beam measured without sample using the same experimental parameters as for I^+ and I^-.

To calculate spin and orbital moments from the transmission data by means of sum-rule analysis[17], the linear x-ray absorption coefficients μ^+ and μ^- of the samples are calculated from I^+, I^- and I_0. The transmitted intensity $I^\pm$ of x-rays passing a sample of thickness d is given by[18]

$$I^\pm = I_0 \times exp(-\mu^\pm \times d). \quad (1)$$

Therefore, the linear x-ray absorption coefficient $\mu^\pm$ is given by

$$\mu^\pm \propto -ln(\frac{I^\pm}{I_0}). \quad (2)$$

If interactions among the atoms in the samples can be neglected, the absorption coefficient is proportional to $\sum_i X_i\sigma_{ai}$, where X_i is the relative concentration of atom i in the sample and σ_{ai} its total atomic absorption cross section. This approximation is applicable sufficiently far away from the absorption edges and for photon energies above 30eV[18]. To extract the spin and orbital magnetic moments m_{spin} and m_{orb} the XMCD sum-rules[17] can be used (while neglecting the spin magnetic dipole term $< T_Z >$):

$$m_{orb} = -\frac{N_h}{Pcos\theta}\frac{4q}{3r} \quad (3)$$

$$m_{spin} = -\frac{N_h}{Pcos\theta}\frac{(6p-4q)}{r} \quad (4)$$

with the circular polarization degree P, the number of unoccupied 3d states N_h, and the angle θ between magnetization and x-ray beam direction. The integrals p, q and r are defined as

$$p = \int_{L_3}(\mu^+ - \mu^-)dE$$
$$q = \int_{L_3+L_2}(\mu^+ - \mu^-)dE$$
$$r = \int_{L_3+L_2}(\mu^+ + \mu^- - 2S)dE$$

The background S is often assumed as a no-free-parameter two-step-like function[17] with thresholds set to the peak positions of the L_3 and L_2 white lines and step heights of 2/3 (L_3) and 1/3 (L_2) of the average absorption coefficient in the post-edge region ("post-edge jump height η"). However, the application of sum-rules requires the knowledge of the number of holes N_h. Usually the number is taken from band-structure calculations. But as discussed above since different crystal structures have been proposed for CoMnSb, we follow the approach by Stöhr *et al.*[19]. They showed that the integral r is proportional to N_h: $r = CN_h\eta$. The constant C depends on the transition matrix elements connecting the core and valence states involved in the $2p$ to $3d$ transitions. Scherz[20] analyzed the $L_{2,3}$ edge XA spectra of $3d$ transition metals from Ti to Ni, with exception of Mn, in detail. Especially, he determined the ratio of r and N_h for normalized (i.e., $\eta = 1$) XA spectra. For Co he found $C^{Co} = 7.8$eV. Although not investigated experimentally by Scherz we can estimate the constant for Mn as $C^{Mn} = 6.0$eV by fitting his results for the other $3d$ transition metals ($C^{Ti} = 5.4$eV, $C^V = 5.3$eV, $C^{Cr} = 5.7$eV, $C^{Fe} = 6.6$eV, $C^{Co} = 7.8$eV and $C^{Ni} = 8.1$eV) by a polynomial.

In our Co-Mn-Sb compounds the post-edge jump heights $\eta^{Co,Mn}$ of Co and Mn in an XA spectrum depend on the Mn and Co concentration X_i and on the total atomic absorption cross section σ_{ai}. The Co and Mn concentrations are known for our films sputtered from different targets. The cross sections can be taken from the Henke tables[21]. The resulting ratios of the post-edge jump heights are $\eta^{Co}/\eta^{Mn} = 0.806$ for sample I , 0.935 for sample II and 1.120 for sample III, respectively.

Taking the relation $r = CN_h\eta$ into account we can substitute the pre-factor N_h/r in Eq. 3 and 4 and get

$$m^i_{orb} = -\frac{\alpha_i}{C^i\eta^i Pcos\theta}\frac{4q_i}{3} \quad (5)$$

$$m^i_{spin} = -\frac{\alpha_i}{C^i \eta^i P cos\theta}(6p_i - 4q_i) \quad (6)$$

where the index i stands for Co or Mn and the additional constant α_i results from the normalization of the transmission spectra (and, accordingly, of the integrals p_i and q_i) with respect to the absolute values of the absorption coefficients μ^+ and μ^- (see Eq. 2). This constant is the same for Co and Mn in a single measurement and, therefore, cancels out when the spin to orbital moment ratios and ratios of the Co to Mn magnetic moments are calculated for the individual samples. Furthermore, the spin to orbital moment ratios of Co and Mn do not even depend on C^{Co} and C^{Mn}, respectively. Finally, please note that for Mn the jj-mixing can not be neglected[22,23], which is not included in the XMCD sum rules. Following the approach described by Yonamoto *et al.*[23] all Mn spin moments throughout this paper have been multiplied by a compensation factor of $\chi = 1.5$ to take the jj-mixing into account.

III. RESULTS AND DISCUSSION

The contribution of spin and orbital magnetic moments of Co and Mn to the total magnetic moment of the samples was investigated by XA spectroscopy and XMCD. Typical XA spectra of Co and Mn are shown in Fig. 1. Especially, the shape of the Co spectra significantly differs from Co metal[17] and the full Heusler alloy Co_2MnSi[24]. As marked by arrows in Fig. 1(b) two features were found on the high energy side of the L_3 resonance suggesting significant differences in the electronic structure of the unoccupied $3d$ states compared to pure Co metal and Co in Co_2MnSi.

A comparison of the XMCD spectra for sample I, II and III is shown in Fig. 2, with the help of Eq. 5 and 6 the orbital and spin magnetic moment ratio can be calculated from these spectra: The shape of the Mn XMCD asymmetry is nearly the same for all samples, whereas the Mn orbital moment is nearly vanishing (sample I: $m^{Mn}_{orb}/m^{Mn}_{spin}$=-0.6%, sample II: $m^{Mn}_{orb}/m^{Mn}_{spin}$=-2.1%, sample III: $m^{Mn}_{orb}/m^{Mn}_{spin}$=+0.7%) and the Co orbital moment is also very small (sample I: $m^{Co}_{orb}/m^{Co}_{spin}$=+0.1%, sample II: $m^{Co}_{orb}/m^{Co}_{spin}$=+5.3%, sample II: $m^{Co}_{orb}/m^{Co}_{spin}$=+5.6%). Therefore the total magnetic moment of the sample is dominated by the Co and Mn spin moments, which are aligned parallel for all samples. By normalizing both the Mn and the Co XMCD spectra to the maximal XMCD signal at the Mn-L_3 edge for all samples in Fig. 2(a) and (b), the size of the Co XMCD signal is a measure for the ratio of the Co to Mn magnetic moment in the compound. Obviously, the relative contribution of the Co magnetic moment to the total magnetic moment of the samples increases with increasing Co concentration in the films. Naturally, this results partly from the the higher Co concentration of sample II and III compared to sample I, but the spin moment ratio *per atom*

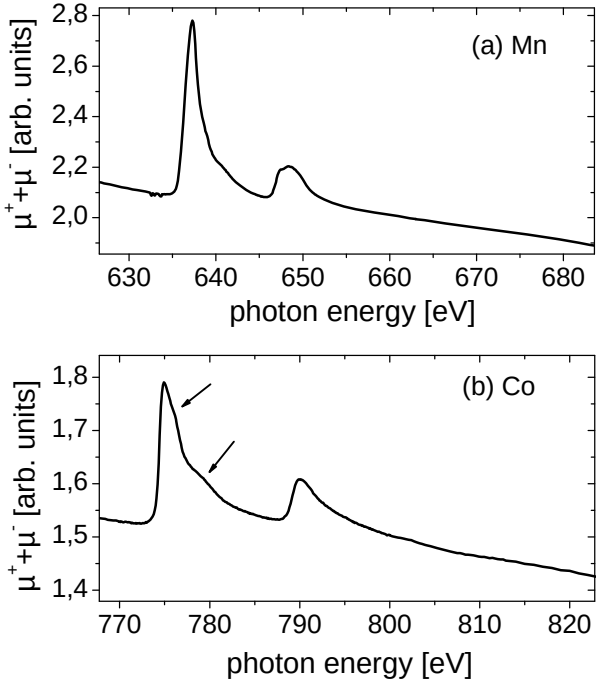

FIG. 1: XA spectra for sample I. The measurements were taken at 295K at normal incidence of the x-rays and an out-of-plane magnetic field of $\pm 0.53T$ (see arrows in Fig. 4) at BL 4.0.2.: (a) XA spectra at the Mn-$L_{2,3}$ edge. (b) XA spectra at the Co-$L_{2,3}$ edge.

of Co to Mn also increases significantly with increasing Co concentration, namely from $m^{Co}_{spin}/m^{Mn}_{spin}$=16.7% for sample I to $m^{Co}_{spin}/m^{Mn}_{spin}$=21.9% for sample II and $m^{Co}_{spin}/m^{Mn}_{spin}$=31.6% for sample III, respectively.

Especially, the shape of the Co XMCD spectra showing the unusual double peak structure at the $L_{2,3}$ edges (see Fig. 2b, the peaks at the L_3 and L_2 edges are marked by "A" / "B" and "C" / "D") changes with different film composition. The intensity of peak "A" is reduced in comparison to "B" with decreasing Co concentration, the same holds for the corresponding peaks "C" and "D" at the L_2 edge. This hints to two non-equivalent Co positions in the Co-Mn-Sb crystal lattice. As discussed in Sec. I different crystal structures should lead to different alignments of the Mn and Co spin moments. We observed a ferromagnetic coupling of the Mn and Co spin moment for all samples. In contrast, for stochiometric CoMnSb crystallized in the $C1_b$ structure - half-metallicity with a *large* spin-down gap is only predicted[9] for this structural type - one would expect an anti-ferromagnetic coupling of Co and Mn spin moments ($m^{Co}_{spin}/m^{Mn}_{spin} = -4.1\%$). For the more complex structure (space group $Fd\bar{3}m$) assumed by Tobola *et al.*[11] resulting in a narrow spin-down gap (but half-metallic character) the calculated ratio of the ferromagnetically coupled Co and Mn mean magnetic moments is +13.7%. Even for crystal structures for which the half-metallicity disappears magnetic mo-

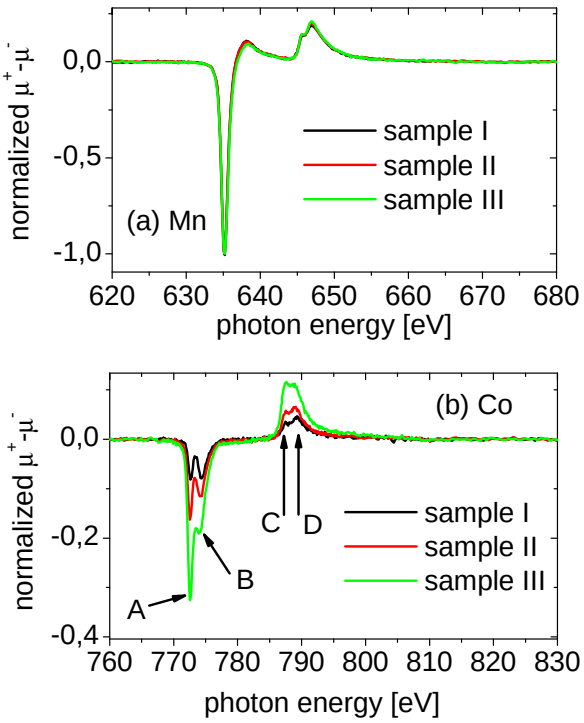

FIG. 2: XMCD spectra for sample I (at 16K), sample II (15K) and sample III (295K) measured at BL 6.3.1: (a) XMCD spectra at the Mn-$L_{2,3}$ edge. (b) XMCD spectra at the Co-$L_{2,3}$ edge. The Mn and Co spectra are normalized to the maximal XMCD signal at the Mn-L_3 edge for each sample. The x-rays angle of incidence was 45^o, the magnetic field was $\pm$ 0.2T and applied parallel to the incident x-ray beam.

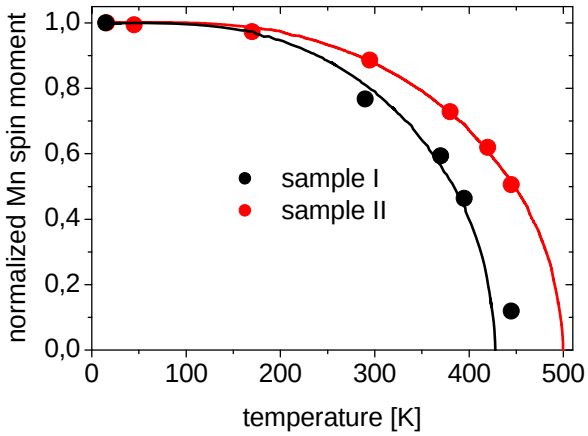

FIG. 3: Temperature dependence of the normalized Mn spin moment of sample I and II measured at BL 6.3.1. The black (red) line corresponds to the temperature dependence of the magnetization expected from the mean-field approximation ($J = 1$) for a critical temperature of $T_C = 430$K ($T_C = 500$K). The x-rays angle of incidence with respect to the sample surface was 45^o, the magnetic field was $\pm$ 0.2T and applied parallel to the incident x-ray beam.

ment ratios have been calculated which fit much better to our experimental result than the results for the ideal $C1_b$ structure[9], namely +8.3% for a disordered $L2_1$ structure[13] and 15.8% for an alternation of Co_2MnSb and MnSb structural units[14], which is closest to our experimental value of $m^{Co}_{spin}/m^{Mn}_{spin}$=16.7% measured at BL 6.3.1 for sample I. Therefore our XMCD results suggest, that even the nearly stochiometric Co-Mn-Sb films (sample I) are crystallized in a non-ideal structure and not in the ideal $C1_b$ structure, which would be the preferred phase regarding the predicted electronic properties.

Because the magnetic spin moment per atom of pure Co metal ($m^{Co}_{spin} \approx 1.6\mu_B$[17]) is considerably larger than the Co spin moments predicted for CoMnSb (see Sec. I and above) one would expect that additional Co atoms - which tend to couple ferromagnetically to nearest-neighbor Co atoms - should have an increased spin moment. This expectation is in qualitative agreement with the observed increasing $m^{Co}_{spin}/m^{Mn}_{spin}$ ratios, if one compares the nearly stochiometric sample I with the off-stochiometric samples II and III.

The temperature dependence of the Mn spin moment was investigated for sample I and II (see Fig. 3). The black and red lines in Fig. 3 correspond to the temperature dependencies expected from simple mean-field theory with $J = 1$. From this the critical temperatures of sample I and sample II can be estimated to be 430K and 500K, respectively, which is comparable to the the Curie temperatures reported for bulk CoMnSb samples (T_C ranges from 474K to 490K[14,25,26]).

Because of the relatively low critical temperature of sample I we could determine the ratio of the Mn to Co spin moments with high accuracy even for temperatures close to T_C at BL 4.0.2. As shown in Fig. 4 the hysteresis loop shape changes significantly at temperatures close to T_C: Because of the demagnetizing field the out-of-plane direction is an hard axis for the sample I sample measured at 295K (see red curve in Fig. 4). The film is nearly saturated at the maximal magnetic fields of $\pm$0.68T. The corresponding in-plane magnetization curve (see blue curve in Fig. 4) shows a sharp switching around zero-magnetic field, as expected for a magnetization reversal in an easy axis direction. At 450K we found a paramagnetic loop shape for in-plane as well as out-of-plane magnetic field (black curve in Fig. 4), which can be well described by a Langevin function[27] $M = M_S(\coth x - x^{-1})$ with $x = \mu_0 H \mu_{para}/k_B T$. Here M_S is the saturation magnetization of the sample, μ_0 the magnetic field constant, k_B the Boltzmann constant, μ_{para} the effective (para)magnetic moment, and T the temperature of the sample. The Langevin fit is shown in green in Fig. 4, the fit parameters are $M(H_{max} = 0.68T)/M_S = 0.684$ and $\mu_{para} = 2944 \pm 71\mu_B$.

The shape of both Mn and Co XMCD spectra does not change at elevated temperatures which can be seen in

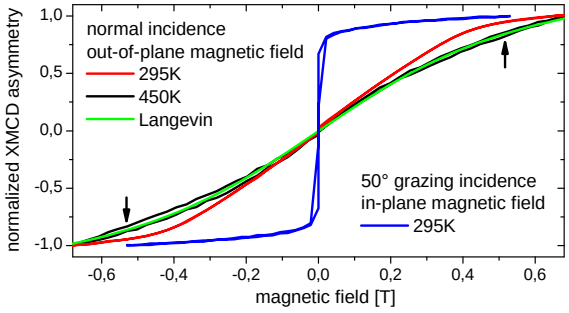

FIG. 4: Hysteresis loops of sample I measured at BL 4.0.2. The black and the red curve are the normalized XMCD asymmetries measured at 450K and 295K for normal incidence of the x-rays and an out-of-plane magnetic field, the x-ray beam and the magnetic field were aligned parallel. The normalized XMCD asymmetry for 50^o grazing incidence of the x-rays and a magnetic field applied in the sample plane is shown in blue. The loops are extracted from the transmitted intensity at the photon energy of 637.0eV with maximal XMCD signal of the Mn-L_3 edge, see Fig. 5a, for left and right elliptically polarized light and different magnetic field values H. The normalized XMCD asymmetry for a certain magnetic field H is given by calculating $[I(P=+0.9,H)-I(P=-0.9,H)]/[I(P=+0.9,H)+I(P=-0.9,H)]$ first and by normalizing the result to a range of [-1, +1] afterwards.

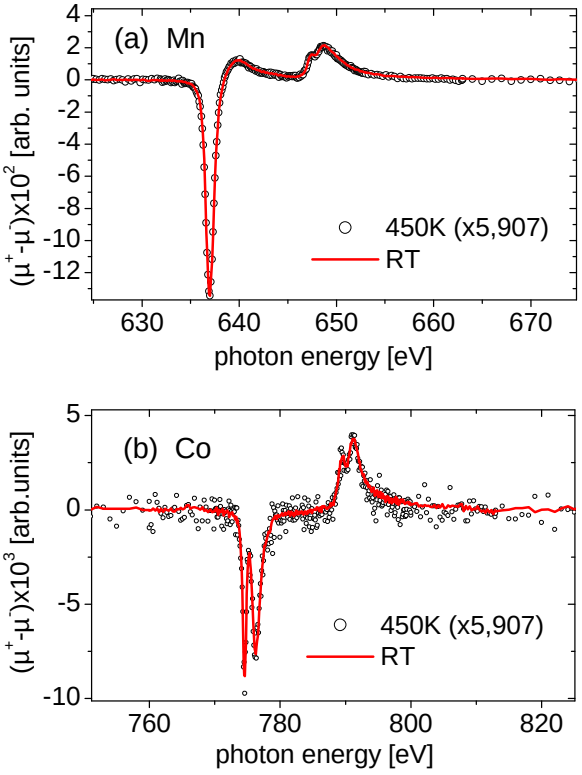

FIG. 5: XMCD spectra for sample I corresponding to the XA shown in Fig. 1. The measurements are taken at 295K and 450K with normal incidence of the x-rays and an out-of-plane magnetic field of $\pm 0.53T$ at BL 4.0.2. The shown data are the average of subsequently taken spectra using left and right elliptically polarized x-rays, respectively: (a) XMCD spectra at the Mn-$L_{2,3}$ edge. (b) XMCD spectra at the Co-$L_{2,3}$ edge. The spectra taken at 450K are multilpied by a factor of 5.9.

Fig. 5 showing spectra taken at 295K and 450K. As mentioned above a temperature of 450K is close to the Curie temperature T_C of sample I, which results in a strong reduction of the magnetization of the sample and, accordingly, the XMCD signal (the 450K spectra are scaled by a factor of 5.9 for better comparability with the 295K measurements). The unchanged shape and the same scaling factors for Mn and Co as well show, that the spin to orbital moment ratio for Co and Mn, respectively, does not change. Furthermore, the ratio of the Mn to Co magnetic moments stays constant up to temperatures close to T_C. Finally, we have to mention that we found some differences of the shape of the XMCD asymmetries for Co and Mn measured at BL 4.0.2 (see Fig. 5) in normal incidence and at BL 6.3.1 (see Fig. 2) with 45^o grazing incidence. This results in somewhat different values for the orbital to spin moment ratios and the Co to Mn spin moment ratio extracted from Fig. 5 ($m_{orb}^{Mn}/m_{spin}^{Mn}$=0.4%, $m_{orb}^{Co}/m_{spin}^{Co}$=2.2% and $m_{spin}^{Co}/m_{spin}^{Mn}=11.8\%$) compared to the above mentioned values. The reason for this is not clear at the moment, it might be connected to the different measurement geometry or to differences in the energy resolution of BL 6.3.1 and BL 4.0.2.. However, the most important result with respect to the electronic structure of our Co-Mn-Sb films, namely the ferromagnetic coupling of the Mn and Co spin moments is not affected by these differences.

IV. CONCLUSION

The influence of the stochiometry of magnetron sputtered thin Co-Mn-Sb films with composition $Co_{32.4}Mn_{33.7}Sb_{33.8}$, $Co_{37.7}Mn_{34.1}Sb_{28.2}$ and $Co_{43.2}Mn_{32.6}Sb_{24.2}$ on their element-specific magnetic properties has been investigated. In general the orbital magnetic moments per atom of Mn and Co are very small compared to the spin magnetic moments for all samples and the Co and Mn spin moments are ferromagnetically coupled. The latter suggests, that even the nearly stochiometric $Co_{32.4}Mn_{33.7}Sb_{33.8}$ films are not crystallized in the $C1_b$ structure which is predicted to show an antiferromagnetic coupling of the Mn and Co spin moment and to have the most suitable electronic properties for spintronics applications, namely half-metallicity with a large gap in the density states of the minority electrons. The relative contribution of the total Co spin moment to the overall magnetic moment of the samples increases with increasing Co content in the film due to the higher

Co concentration and also from a higher spin moment per Co atom compared to the Mn atoms. The estimated critical temperatures of the $Co_{32.4}Mn_{33.7}Sb_{33.8}$ (about 430K) and $Co_{37.7}Mn_{34.1}Sb_{28.2}$ (about 500K) films are consistent with the Curie temperatures observed for CoMnSb bulk samples. The temperature dependent element-specific properties of the $Co_{32.4}Mn_{33.7}Sb_{33.8}$ films have been investigated in detail up to 450K, e.g., close to T_C. The shape of the XMCD asymmetries of Mn and Co did not changed at this temperature, therefore, the orbital to spin moment ratios of Co and Mn as well as the ratio of the Co to Mn spin moment ratio are not changed at this high temperature.

Acknowledgment

The authors gratefully acknowledge financial support by the Deutsche Forschungsgemeinschaft (DFG) and the opportunity to work at BL 6.3.1 and BL 4.0.2 of the Advanced Light Source, Berkeley, USA, which is supported by the Director, Office of Science, Office of Basic Energy Sciences, of the U.S. Department of Energy under Contract No. DE-AC02-05CH11231. Furthermore, we like to thank N. N. Liu for assisting the sample preparation. One of the authors (M. M.) acknowledges the Deutsche Akademische Auslandsamt (DAAD) for supporting his work at AGH Krakow.

---

* Electronic address: jschmalh@physik.uni-bielefeld.de

[1] S. A. Wolf, D. D. Awschalom, R. A. Buhrman, J. M. Daughton, S. von Molnar, M. L. Roukes, A. Y. Chtchelkanova, and D. M. Treger, Science **294**, 1488 (2001).
[2] G. Reiss and D. Meyners, Appl. Phys. Lett. **88**, 043505 (2006).
[3] A. Thomas, D. Meyners, D. Ebke, N. Liu, M. D. Sacher, J. Schmalhorst, G. Reiss, H. Ebert, and A. Hütten, Appl. Phys. Lett. **89**, 012502 (2006).
[4] R. de Groot, F. Mueller, P. van Engen, and K. Buschow, Phys. Rev. Lett. **50**, 2024 (1983).
[5] S. Ishida, T. Masaki, S. Fujii, and S. Asano, Physica B **245**, 1 (1998).
[6] I. Galanakis, P. H. Dederichs, and N. Papanikolaou, Phys. Rev. B **66**, 174429 (2002).
[7] S. Wurmehl, G. Fecher, H. C. Kandpal, V. Ksenofontov, C. Felser, H.-J. Lin, and J. Morais, Phys. Rev. B **72**, 184434 (2005).
[8] *Half-metallic Alloys: Fundamentals and Application*, I. Galanakis and P. H. Dedrichs (Eds.), Lecture Notes in Physics 676, Springer Berlin Heidelberg (2005), ISBN-10 3-540-27719-6.
[9] I. Galanakis, J. Phys.: Condens. Matter **14**, 6329 (2002).
[10] M. J. Otto, H. Feil, R. A. M. van Woerden, J. Wijngaard, P. J. van der Valk, C. F. van Bruggen, and C. Haas, J. Magn. Magn. Mat. **70**, 33 (1987).
[11] J. Tobola and J. Pierre, J. Alloys and Compd. **296**, 243 (2000).
[12] J. P. Senateur, A. Rouault, R. Fruchart, and D. Fruchart, J. Solid State Chem. **5**, 226 (1972).
[13] K. Kaczmarska, J. Pierre, J. Tobola, and R. V. Skolozdra, Phys. Rev. B **60**, 373 (1999).
[14] V. Ksenofotov, G. Melnyk, M. Wojcik, S. Wurmehl, K. Kroth, S. Reimann, P. Blaha, and C. Felser, Phys. Rev. B **74**, 134426 (2006).
[15] The annealing temperature was optimized by measuring the magnetization of sample II like Cu^{80nm} / $Ta^{2.5nm}$ / V^{10nm} / Co-Mn-Sb^{20nm} (target II) / $Al^{1.6nm}$ stacks grown on Si(100)-wafer capped by SiO_2^{50nm} instead of Si_3N_4-membranes after annealing at temperature between 200°C and 400°C. A maximum magnetization of 461 kA/m was found after annealing at 300°C.
[16] Y. U. Idzerda, C. T. Chen, H.-J. Lin, G. Meigs, G. H. Ho, and C.-C. Kao, Nucl. Instrum. Methods Phys. Res. A **347**, 134 (1994).
[17] C. T. Chen, Y. U. Idzerda, H.-J. Lin, N. V. Smith, G. Meigs, E. Chaban, G. H. Ho, E. Pellegrin, and F. Sette, Phys. Rev. Lett. **75**, 152 (1995).
[18] A. Thomson, D. Attwood, E. Gullikson, M. Howells, J. Kortright, A. Robinson, J. Underwood, K.-J. Kim, J. Kirz, I. Lindau, et al., X-ray Data Booklet, Lawrence Berkeley National Laboratory, http://xdb.lbl.gov.
[19] J. Stöhr, J. Elect. Spect. Rel. Phen. **75**, 253 (1995).
[20] A. Scherz, PhD thesis, Freie Universitaet Berlin (2003), see Table 3.1.
[21] The Henke tables can be found, e.g., at http://henke.lbl.gov/optical_constants/filter2.html.
[22] H. A. Dürr, G. van der Laan, D. Spanke, F. U. Hillebrecht, and N. B. Brookes, Phys. Rev. B **56**, 8156 (1997).
[23] Y. Yonamoto, T. Yokoyama, K. Amemiya, D. Matsumura, and T. Ohta, Phys. Rev. B **63**, 214406 (2001).
[24] J. Schmalhorst, S. Kämmerer, M. Sacher, G. Reiss, A. Hütten, and A. Scholl, Phys. Rev. B **70**, 024426 (2004).
[25] S. Li, M. Liu, Z. Huang, F. Xu, W. Zou, F. Zhang, and Y. Du, J. Appl. Phys. **99**, 063901 (2006).
[26] K. H. J. Buschow, P. G. van Engen, and R. Jongebreur, J. Magn. Magn. Mat. **38**, 1 (1983).
[27] P. Langevin, Annales de Chemie et de Physique **5**, 70 (1905).